Strength of FRP RC sections after long-term loading

M. A. Pisani†

*Politecnico di Milano, Department of Structural Engineering, Piazza Leonardo da Vinci 32,
20133 Milan, Italy*

Abstract. The adoption of fibre reinforced polymer (FRP) rebars (whose behaviour is elastic-brittle) in reinforced concrete (RC) cross sections requires the assessment of the influence of time-dependent behaviour of concrete on the load-carrying capacity of these sections. This paper presents a method of computing the load-carrying capacity of sections that are at first submitted to a constant long-term service load and then overloaded up to ultimate load. The method solves first a non-linear visco-elastic problem, and then a non-linear instantaneous analysis up to ultimate load that takes into account the self-equilibrated stress distribution previously computed. This method is then adopted to perform a parametric analysis that shows that creep and shrinkage of concrete increase the load-carrying capacity of the cross section reinforced with FRP and allows for the suggestion of simple design rules.

Key words: RC; compact cross-sections; long-term loading; load-carrying capacity; FRP reinforcement.

1. Introduction

The adoption of fibre reinforced polymer (FRP) rebars and cables in reinforced concrete (RC) and prestressed concrete (PC) compact cross sections seems promising to solve durability problems related to extreme environment conditions (marine environment, cold regions). Generally speaking, the hope of the researchers is to solve the problem related to corrosion of steel in every environment, but a lot of work still has to be done to achieve this target.

The overall behaviour at ultimate of concrete sections reinforced or prestressed with FRP rebars and cables is one of the subjects under discussion.

Dealing with the load-carrying capacity of RC and PC sections after long-term loading, CEB (1984) quotes "It may be easily verified that the influence of time-dependent behaviour must be considered essentially in the safety-checks of concrete structures with respect to serviceability. On the contrary - as it is the case for the effect of other imposed deformations e.g., due to thermal effects - the influence of creep and shrinkage is largely reduced when an ultimate limit state is approached due to the appearance of large inelastic deformations in both materials". This is a statement generally accepted when dealing with steel reinforcement, but it has to be assessed when adopting FRP, whose behaviour is linear up to collapse, at least if dealing with carbon (CFRP), aramid (AFRP) or glass (GRFP) fibres, which are the fibres currently used to make rebars and wires.

---

† Associate Professor

For sake of completeness it has to be mentioned that some research teams are investigating the possibility of designing FRP rebars, made by coupling distinct reinforcing fibres, whose overall behaviour looks similar to that of a steel rebar under a monotonic load increase (see Malvar 1994, Tepfers *et al.* 1999). Other fibres, besides those previously mentioned, are being investigated to make the fibre reinforcement in FRP rebars and wires (e.g., basalt fibres, see Jung and Subramanian 1994). In any case no commercial product of this kind is at present available, and therefore this paper will not deal with them.

This paper suggests a numerical method conceived to analyse the behaviour of compact RC cross sections reinforced with steel or FRP rebars. This method solves first a non-linear visco-elastic problem (RC cross section under sustained loads), and then a non-linear instantaneous analysis up to ultimate load that takes into account the self-equilibrated stress distribution previously computed.

The numerical method is then adopted to perform a parametric analysis whose aim is to determine whether the self-equilibrated stress distribution that is caused by creep and shrinkage of concrete changes the load-carrying capacity of a RC section reinforced with FRP and, if so, what is its maximum extent, in order to assess if it has to be taken into account in common practice. To achieve this target, RC sections are analysed under constant service loads, which are increased up to collapse after 150 years.

The investigation is only numerical, but it is based on constitutive laws recommended by widely accepted codes of practice. Moreover, numerical analysis allows avoiding all the uncertainties related to the preparation and execution of a large number of experimental tests that should differ from one another just in one parameter, and it is inexpensive since an experimental test would last at least ten years in a climatic chamber.

2. Constitutive laws of the materials

As pointed out earlier, this study deals with commercial FRP rebars made with one of the following fibres: carbon, aramid or glass.

Aramid fibres bring with them a marked relaxation that modifies the self-equilibrated stress distribution that springs from creep and shrinkage of concrete. The interaction between the delayed behaviour of concrete and of the reinforcement is complicated even when dealing with uncracked sections, that is prestressed and partially prestressed cross sections (see Pisani 2000). Moreover, the relaxation law of AFRP reinforcement embedded in concrete is still not well known. On the contrary, relaxation of CFRP and GFRP cables is well established and similar to that of steel strands (lower than 3%), that is it is not significant when these materials are adopted to make rebars. These remarks suggested not taking into account AFRP in this study.

The constitutive law adopted for steel rebars (CEN 1991, CEB-FIP 1991) is represented in Fig. 1(c):

$$\begin{cases} \sigma_s = \varepsilon_s \cdot E_s^{\text{sec}}(\varepsilon_s) \\ E_s^{\text{sec}}(\varepsilon_s) = \begin{cases} f_y/\varepsilon_y & \text{if} \quad -\varepsilon_y \le \varepsilon_s \le \varepsilon_y \\ f_y/\varepsilon_s & \text{if} \quad \varepsilon_y \le |\varepsilon_s| \le \varepsilon_{su} \end{cases} \end{cases} \tag{1}$$

where f_y is the yielding stress, ε_y is the yielding strain and ε_{su} is the ultimate strain.

The mechanical properties of CFRP and GFRP rebars are not yet standardized (commercial
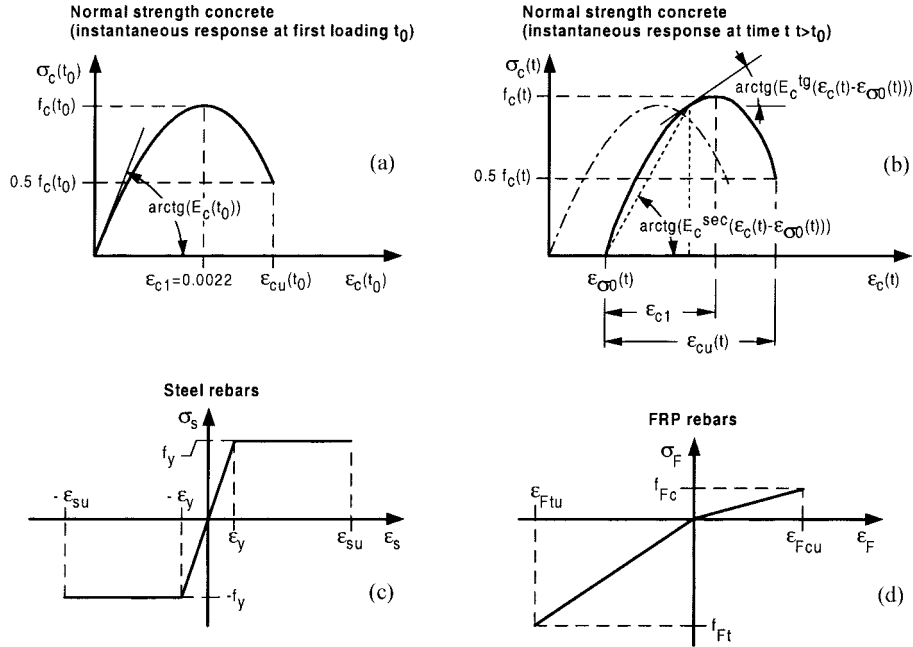
Fig. 1 Instantaneous constitutive laws of concrete, steel and FRP

products of this kind are markedly different from one another) and therefore some comments are needed. The constitutive laws adopted are linear elastic up to collapse (see for instance Erki *et al.* 1993, Machida 1993, Nanni 1993, Agarwal *et al.* 1994), but their elastic tensile modulus and their strength are usually different form those measured under compression (compressive stresses are assumed positive):

$$
\begin{cases}
\sigma_F = \varepsilon_F \cdot E_F^{sec}(\varepsilon_F) \\
E_F^{sec}(\varepsilon_F) = \begin{cases} f_{Fc}/\varepsilon_{Fcu} & \text{if} \quad 0 \le \varepsilon_F \le \varepsilon_{Fcu} \\ f_{Ft}/\varepsilon_{Ftu} & \text{if} \quad \varepsilon_{Ftu} \le \varepsilon_F \le 0 \end{cases}
\end{cases}
\tag{2}
$$

where f_{Fc} and ε_{Fcu} are respectively the compressive strength and the ultimate compressive strain, whereas f_{Ft} and ε_{Ftu} are the tensile ones (Fig. 1d).

Dealing with Durglass FL $\varnothing$ 10 mm, a bar whose tensile strength f_{Ft} is about 1000 MPa, a number of tests (nine tensile tests and nine compressive tests) were performed to measure the compressive strength f_{Fc} (according to ASTM D659M-91), the elastic moduli both under tension and compression and the Poisson's ratio v_{Ft}. The outcome is briefly summarized in Table 1.

Other rebars (e.g., those tested by Chaallal *et al.* 1993, and Benmokrane *et al.* 1996) have different compressive and tensile strength but, owing to the application of helically wounded glass fibre embossment, they show almost the same modulus of elasticity under tension and compression. This comparison shows how the manufacturing technique, together with the type and diameter of the fibres, the type of the resin and the fibre volume fraction, influence the overall behaviour of the rebar.

Table 1 Mechanical properties of Durglass FL $\varnothing$ 10 mm

	Tension characteristics (nine tests)		Compression characteristics (nine tests)	
	Elastic modulus [N/mm²]	Poisson's ratio ν_{Ft} [N/mm²]	Elastic modulus [N/mm²]	Strength f_{Fc} [N/mm²]
Mean value	43707	0.31	27133	384.8
Standard deviation	468	0.02	484	31.9

No relaxation will be taken into account for both steel and composite rebars as they are similar to one another. In any case, relaxation of the steel rebars is not usually taken into account.

In common practice, the constitutive law that applies to concrete depends on the type of safety-check that is going to be performed. Bending of a PC compact cross section is usually checked by means of a linear elastic constitutive law when dealing with instantaneous service loads, or a linear viscoelastic constitutive law if the load is sustained, whereas a constitutive law like the one drawn in Fig. 1(a) (CEB-FIP 1991) is usually adopted in order to check its load-carrying capacity.

As already stated, this paper aims at investigating the behaviour of RC sections that are at first loaded with constant long-term service loads and then instantaneously overloaded up to ultimate. A constitutive law that applies in both stages, i.e., throughout the stress history of the cross section, is therefore needed. A constitutive law of this kind is not available in the European code and therefore an in-depth discussion of every aspect of the problem is needed to justify all the assumptions adopted in the numerical model.

A first problem that arises when the behaviour of a cross section under low and high bending moment is studied concerns the tensile strength of concrete. The constitutive law should allow for the computation of the residual load-carrying capacity of the RC section at the end of the intended life of the structure in the most unfavourable condition. At this stage the structure has experienced more than once the maximum service load it was designed for. Therefore, the structure could probably be cracked in those sections where collapse can occur when instantaneously overloaded (i.e., the sections this work is interested in). The service load history is not known, but the previous statement suggests to ignore the tensile strength of concrete (the maximum service load could occur at time of first loading; crack could also occur because of hydration heat or shrinkage of concrete). Moreover, the constitutive law of concrete has to be consistent at all stress levels. When dealing with the ultimate limit state of bending and compression, it is customary to neglect the tensile strength of concrete. If this tensile strength is neglected when dealing with service loads too, consistency is automatically satisfied.

The compressive instantaneous constitutive law at time of first loading (that is without the effects of creep and shrinkage of concrete) suggested by CEB-FIP (1991) is:

$$\sigma_c(t_0) = \frac{\dfrac{E_c(t_0) \cdot \varepsilon_c(t_0)}{E_{c1}(t_0) \cdot \varepsilon_{c1}} - \left(\dfrac{\varepsilon_c(t_0)}{\varepsilon_{c1}}\right)^2}{1 + \left(\dfrac{E_c(t_0)}{E_{c1}(t_0)} - 2\right) \cdot \dfrac{\varepsilon_c(t_0)}{\varepsilon_{c1}}} \cdot f_{cm}(t_0) \qquad [0 \le \varepsilon_c(t_0) \le \varepsilon_{cu}(t_0)] \qquad (3)$$

where $f_{cm}(t_0)$ is the mean compressive strength of concrete at time t_0 [days] and:

$$\varepsilon_{c1} = 0.0022$$
$$E_{c1}(t_0) = f_{cm}(t_0)/\varepsilon_{c1}$$
$$E_c(t_0) = \text{tangent Young modulus at time } t_0 \text{ (see Eq. (8))}$$
$$\alpha = E_c(t_0)/E_{c1}(t_0)$$

$$\varepsilon_{cu}(t_0) = \varepsilon_{c1}[0.25\alpha + 0.5 + \sqrt{(0.25\alpha + 0.5)^2 - 0.5}] \qquad (4)$$

No safety factor is adopted, owing to the aim of simulating an experimental test.

The coupling of the previous assumptions leads to the following instantaneous constitutive law at time of first loading t_0:

$$
\begin{cases}
\sigma_c(t_0) = E_c^{\text{sec}}(\varepsilon_c(t_0)) \cdot \varepsilon_c(t_0) \\
\\
E_c^{\text{sec}}(\varepsilon_c(t_0)) = \begin{cases}
0 & \text{if} \quad \varepsilon_c(t_0) < 0 \\
\\
\dfrac{\dfrac{E_c(t_0)}{f_{cm}(t_0)} - \dfrac{\varepsilon_c(t_0)}{\varepsilon_{c1}^2}}{1 + \left(\dfrac{E_c(t_0)}{E_{c1}(t_0)} - 2\right) \cdot \dfrac{\varepsilon_c(t_0)}{\varepsilon_{c1}}} \cdot f_{cm}(t_0) & \text{if} \quad 0 \le \varepsilon_c(t_0) \le \varepsilon_{cu}(t_0)
\end{cases}
\end{cases}
\qquad (5)
$$

Eq. (5) implies that the mechanical properties of concrete change with its age. Age of concrete (days after hardening) can therefore be adopted to identify the time-evolution of stress and strain in the RC section, that is it represents also the time-scale of the experiment.

Strength of concrete changes with time. CEB (CEB-FIP 1991, see also CEB 1993) suggests adopting a variable strength whose law depends on the type of cement, temperature and curing conditions. Nevertheless, this stress increase is not taken into account in common practice. Therefore the residual load carrying capacity of RC sections reinforced with FRP after long-term loading will be determined by adopting both a constant strength and a strength increasing with the age of concrete according to:

$$f_{cm}(t) = \beta_{cc}(t) \cdot f_{cm}(28) \qquad (6)$$

where:

$$\beta_{cc}(t) = e^{s\left[1 - \left(\frac{28}{t}\right)^{1/2}\right]} \ ; \ s = \begin{cases} 0.20 & \text{high strength rapid hardening cement} \\ 0.25 & \text{normal hardening and rapid hardening cement} \\ 0.38 & \text{slow hardening cement} \end{cases} \qquad (7)$$

The same code suggests:

$$E_c(t) = \sqrt{\beta_{cc}(t)} \cdot 21500 \cdot \left[\frac{f_{cm}(28)}{10}\right]^{1/3} \quad \text{[MPa]} \qquad (8)$$

to determine the tangent Young modulus at any time [days].

The response of concrete at time t to an instantaneous stress variation depends on the actual mechanical properties of the material. Concrete total strain $\varepsilon_c(t)$ at time t can be described as the sum of the instantaneous response to unloading $\varepsilon_{c,inst}(t)$, plus strain $\varepsilon_{\sigma0}(t)$ that takes into account the

previous loading history, that is:

$$\varepsilon_c(t) = \varepsilon_{c,inst}(t) + \varepsilon_{\sigma0}(t) \tag{9}$$

Strictly speaking, $\varepsilon_{\sigma0}(t)$ is the residual strain (due to creep and shrinkage of concrete) at time t after instantaneous unloading. The instantaneous response at time t is therefore similar to the one described by Eq. (5), provided $\varepsilon_c(t_0)$, $E_c(t_0)$, $E_{c1}(t_0)$ and $f_{cm}(t_0)$ are replaced with $\varepsilon_{c,inst}(t) = \varepsilon_c(t) - \varepsilon_{\sigma0}(t)$, $E_c(t)$, $E_{c1}(t)$ and $f_{cm}(t)$ (see Fig. 1b):

$$\begin{cases} \sigma_c(t) = E_c^{sec}(\varepsilon_c(t) - \varepsilon_{\sigma0}(t)) \cdot [\varepsilon_c(t) - \varepsilon_{\sigma0}(t)] \\[2mm] E_c^{sec}(\varepsilon_c(t) - \varepsilon_{\sigma0}(t)) = \begin{cases} 0 & \text{if} \quad [\varepsilon_c(t) - \varepsilon_{\sigma0}(t)] < 0 \\[3mm] \dfrac{\dfrac{E_c(t)}{f_{cm}(t)} - \dfrac{[\varepsilon_c(t) - \varepsilon_{\sigma0}(t)]}{\varepsilon_{c1}^2}}{1 + \left(\dfrac{E_c(t)}{E_{c1}(t)} - 2\right) \cdot \dfrac{[\varepsilon_c(t) - \varepsilon_{\sigma0}(t)]}{\varepsilon_{c1}}} \cdot f_{cm}(t) & \text{if} \quad 0 \le [\varepsilon_c(t) - \varepsilon_{\sigma0}(t)] \le \varepsilon_{cu}(t) \end{cases} \end{cases} \tag{10}$$

The previous law implies that an infinitesimal, instantaneous compressive stress change at time $t_0 \le \tau \le t$ holds for:

$$d(\varepsilon_c(\tau) - \varepsilon_{\sigma0}(\tau)) = \frac{d\sigma_c(\tau)}{E_c^{tg}(\varepsilon_c(\tau) - \varepsilon_{\sigma0}(\tau))} \tag{11}$$

where $E_c^{tg}(\varepsilon_c(\tau) - \varepsilon_{\sigma0}(\tau))$ is the tangent modulus at the actual (at time τ) strain level.

It is generally assessed that if the maximum sustained compressive stress in concrete does not exceed $0.4 \cdot f_{cm}(28)$ (CEB-FIP 1991, CEB 1993), creep strain can be fairly well approximated by a linear function of the instantaneous stress variation and McHenry superposition principle applies, that is ($\varepsilon_{sh}(t)$ is the shrinkage strain):

$$\varepsilon_c(t) = \sigma_c(t_0) \cdot J(t, t_0) + \int_{t_0}^{t} d\sigma_c(\tau) \cdot J(t, \tau) + \varepsilon_{sh}(t)$$

$$= \sigma_c(t_0) \cdot \frac{[1 + \varphi(t, t_0)]}{E_c(t_0)} + \int_{t_0}^{t} d\sigma_c(\tau) \cdot \frac{[1 + \varphi(t, \tau)]}{E_c(\tau)} + \varepsilon_{sh}(t) \tag{12}$$

where $J(t, \tau)$ stands for the creep function and $\varphi(t, \tau)$ is the creep coefficient.

This constitutive law implies a linear instantaneous behaviour. When applying this rule to a non-linear instantaneous constitutive law of the same material, under the same upper limitation of the maximum compressive stress, remembering Eq. (11), the constitutive law of compressed concrete under sustained loads becomes:

$$\varepsilon_c(t) = \frac{\sigma_c(t_0)}{E_c^{sec}(\sigma_c(t_0))} \cdot [1 + \varphi(t, t_0)] + \int_{t_0}^{t} \frac{d\sigma_c(\tau)}{E_c^{tg}(\sigma_c(\tau))} \cdot [1 + \varphi(t, \tau)] + \varepsilon_{sh}(t)$$

$$0 \le \sigma_c(\tau) \le 0.4 \cdot f_{cm}(28) \quad \forall \tau: t_0 \le \tau \le t \tag{13}$$

Eq. (10) implies that the relation between instantaneous strain and stress is unique. Nevertheless, when dealing with the compressive stress range $0 \leq \sigma_c(\tau) \leq 0.4 \cdot f_{cm}(28)$ (see Eq. (13)), the same relation is biunique and hence the tangent and secant elastic moduli in Eq. (13) can be written as functions of the compressive stress.

To be consistent with Eq. (10), creep coefficient and shrinkage strain can be calculated through the equations suggested by CEB (CEB-FIP 1991). These equations are well established, reliable and adopted by the European code. More refined equations could be adopted as well, as far as a non-linear instantaneous, linear visco-elastic constitutive law can be built with them, but it is felt that they would not change the results of the investigation.

The upper limits imposed by the codes to maximum service stresses suggest adopting $0.3 \cdot (f_{cm}(28) - 8)$ [MPa] as an upper bound of the real sustained stress acting on usual structures (according to CEB 1991, and CEN 1991, concrete design strength is equal to $0.57 \cdot (f_{cm}(28) - 8)$ [MPa]). At these low levels of stress, the error gathered when substituting the secant and tangent moduli with the tangent modulus at $\varepsilon_c = 0$ (see Eq. (8)) is negligible, and therefore Eq. (13) can be replaced by Eq. (12). If so, the instantaneous constitutive law of concrete under long-term load becomes:

$$
\begin{cases}
\sigma_c(t) = E_c(t) \cdot [\varepsilon_c(t) - \varepsilon_{\sigma 0}(t)] & \text{if} \quad [\varepsilon_c(t) - \varepsilon_{\sigma 0}(t)] \geq 0 \\
\sigma_c(t) = 0 & \text{if} \quad [\varepsilon_c(t) - \varepsilon_{\sigma 0}(t)] \leq 0
\end{cases}
\tag{14}
$$

Owing to the lack of strength of concrete under tension, the coupling of Eq. (12) and Eq. (14) is a linear visco-elastic, non-linear instantaneous constitutive law.

Eq. (12) is a Volterra integral equation. Since the creep law herein adopted (CEB-FIP 1991) is described through the creep function whereas the relaxation function has to be computed case by case by means of numerical integration (as long as the analytical solution is not known), a numerical method to transform Eq. (13) in an algebraic equation is needed. The method adopted (Pisani 1994) makes use of a Gauss quadrature formula. Eq. (13) becomes:

$$
\varepsilon_c(t_k) = \sigma_c(t_0) \cdot J(t_k, t_0) + \sum_{i=1}^{k-1} \frac{\sigma_c(t_{i+1}) - \sigma_c(t_i)}{2} \cdot \sum_{j=1}^{2} P_j \cdot J(t_k, t_{ij}) + \varepsilon_{sh}(t_k)
$$

$$
[t_0 = t_1; \sigma_c(t_i) \geq 0 \quad \forall i = 1, k]
\tag{15}
$$

where t_i and t_{i+1} are respectively the lower and the upper bound of the i-th time-step (after discretization), t_{ij} is the j-th sampling point inside the i-th time-step and P_j is its weight.

Eq. (15) allows evaluating $\sigma_c(t_k)$:

$$
\sigma_c(t_k) = \sigma_c(t_{k-1}) + \frac{2}{\displaystyle\sum_{j=1}^{2} P_j \cdot J(t_k, t_{k-1j})} \cdot \Bigg\{ \varepsilon_c(t_k) - \sigma_c(t_0) \cdot J(t_k, t_0) + -\varepsilon_{sh}(t_k)
$$

$$
- \sum_{i=1}^{k-2} \frac{\sigma_c(t_{i+1}) - \sigma_c(t_i)}{2} \cdot \sum_{j=1}^{2} P_j \cdot J(t_k, t_{ij}) \Bigg\} \geq 0
\tag{16}
$$

that after setting:

$$E_k^* = \frac{2}{\sum\limits_{j=1}^{2} P_j \cdot J(t_k, t_{k-1j})}$$

$$\sigma_c^*(t_k) = E_k^* \cdot \left\{ \sigma_c(t_0) \cdot J(t_k, t_0) + \varepsilon_{sh}(t_k) + \sum_{i=1}^{k-2} \frac{\sigma_c(t_{i+1}) - \sigma_c(t_i)}{2} \cdot \sum_{j=1}^{2} P_j \cdot J(t_k, t_{ij}) \right\} - \sigma_c(t_{k-1}) \qquad (17)$$

can be briefly written as:

$$\begin{cases} \sigma_c(t_k) = E_k^* \cdot \left[\varepsilon_c(t_k) - \dfrac{\sigma_c^*(t_k)}{E_k^*} \right] & \text{if} \quad \left[\varepsilon_c(t_k) - \dfrac{\sigma_c^*(t_k)}{E_k^*} \right] \geq 0 \\[4mm] \sigma_c(t_k) = 0 & \text{if} \quad \left[\varepsilon_c(t_k) - \dfrac{\sigma_c^*(t_k)}{E_k^*} \right] \leq 0 \end{cases} \qquad (18)$$

Eqs. (17) and (18) allow determining $\sigma_c(t_k)$ when the previous stress history (that is the evolution of stresses and strains from time t_0 to time t_{k-1}) is known.

The time of first loading t_0 is the age of concrete when the first external load starts to act on the structure. Adopting Eq. (12), it is implicitly assumed that shrinkage of concrete does not give rise to stresses in concrete before time t_0, but this is impossible when dealing with heterogeneous cross sections (that is with RC sections). Nevertheless, it has to be mentioned that during the curing of concrete there is a complex interaction between shrinkage, mechanical (indents in the mould) and chemical adhesion with the mould, weak tensile strength of concrete and hydration heat. The aim of this work is anyway to analyse the behaviour of RC sections at ultimate after long-term loading, and therefore the small stress distributions that usually can rise at the very beginning of the life of the structural element (that is before time t_0) can be disregarded.

3. Numerical algorithm

Looking at the compact cross section drawn in Fig. 2, symmetric with respect to the y axis, the equilibrium equations can be written as:

$$\int_{A_c} \sigma_c(t) \cdot dA_c + \sum_{i=1}^{n} \sigma_{ri}(t) \cdot A_{ri} = N(t)$$

$$\int_{A_c} \sigma_c(t) \cdot y \cdot dA_c + \sum_{i=1}^{n} \sigma_{ri}(t) \cdot y_{ri} \cdot A_{ri} = M(t) \qquad (19)$$

where index ri stands for the i-th steel or composite rebar.

The Bernoulli-Navier hypothesis and the hypothesis of perfect bond hold for:
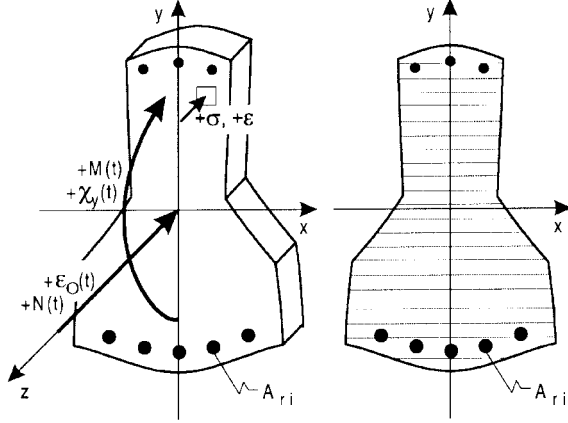
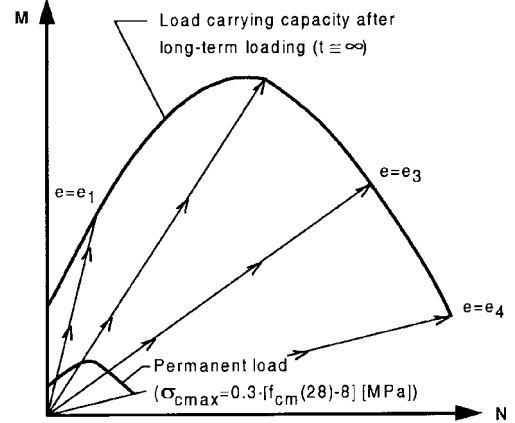Fig. 2 RC cross section and its discretization

Fig. 3 History of loading

$$\varepsilon_c(y, t) = \varepsilon_0(t) + \chi_y(t) \cdot y$$

$$\varepsilon_{ri}(t) = \varepsilon_0(t) + \chi_y(t) \cdot y_{ri} \tag{20}$$

where ε_0 is the strain in the origin of the Cartesian axes and χ_y is the curvature around x axis.

The loading history adopted is illustrated in Fig. 3. It consists in an instantaneous loading at time t_0 up to values that give rise to a maximum stress in concrete equal to $0.3 \cdot (f_{cm}(28) - 8)$ [MPa]. This load is kept constant for about 150 years and then instantaneously increased up to ultimate.

A realistic way to describe the axial force and the bending moment is to keep eccentricity of the load constant all over the loading history. If the axial force or the bending moment were kept constant it would be impossible to determine the branch of the interaction diagram where the specified constant internal action exceeds the maximum value for which $\sigma_{cmax}(t_0) = 0.3 \cdot (f_{cm}(28) - 8)$ [MPa]. Other loading histories are anyway possible.

First of all, the long-term internal actions N_0 and $M_0 = e \cdot N_0$ have to be determined. Owing to the adoption of Eq. (14), the lack of strength of concrete under tension still implies a non-linear problem, but the solution can be assessed through well-known numerical methods since the problem becomes that of a RC cracked section under instantaneous service loads (the unknowns are ε_0, χ_y and N_0 (or M_0 if $N_0 = 0$), while $\varepsilon_{\sigma0} = 0$ and the boundary condition is $\sigma_{cmax}(t_0) = 0.3 \cdot (f_{cm}(28) - 8)$ [MPa]).

The analysis of the cross section behaviour under long-term constant load is performed by substituting Eqs. (18) and (20) into Eq. (19). Note that the strain in every point of the concrete cross section depends on its own stress history that, because of the instantaneous non-linear behaviour, is different from one point to another (it will be shown that the neutral axis moves during long-term loading). A discretization of the concrete cross section in m thin strips, whose strain history has to be recorded in order to apply the second of Eq. (18) (that is to determine $\sigma_c^*(t_k)$), has therefore to be adopted (see Fig. 2). More efficient methods like those by Rotter (1985) and Pisani (1996) do not apply. The solving system becomes:

$$\begin{cases} \displaystyle\sum_{j=1}^{m} \delta_{kj} \cdot [E_k^* \cdot \varepsilon_c(y_j, t_k) - \sigma_c^*(y_j, t_k)] \cdot A_{cj} + \sum_{i=1}^{n} E_r^{\mathrm{sec}}(\varepsilon_{ri}(t_k)) \cdot \varepsilon_{ri}(t_k) \cdot A_{ri} = N_0 \\[4mm] \displaystyle\sum_{j=1}^{m} \delta_{kj} \cdot [E_k^* \cdot \varepsilon_c(y_j, t_k) - \sigma_c^*(y_j, t_k)] \cdot A_{cj} \cdot y_j + \sum_{i=1}^{n} E_r^{\mathrm{sec}}(\varepsilon_{ri}(t_k)) \cdot \varepsilon_{ri}(t_k) \cdot A_{ri} \cdot y_{ri} = M_0 \end{cases} \tag{21}$$

where:

$$\delta_{kj} = \begin{cases} 1 & \text{if} \quad \left[\varepsilon_c(t_k) - \dfrac{\sigma_c^*(t_k)}{E_k^*}\right] > 0 \\[5mm] 0 & \text{if} \quad \left[\varepsilon_c(t_k) - \dfrac{\sigma_c^*(t_k)}{E_k^*}\right] \le 0 \end{cases} \tag{22}$$

that is:

$$\underline{\underline{K}}(\underline{\Psi}(t_k), t_k) \cdot \underline{\Psi}(t_k) \;=\; \underline{Q}_0 + \underline{Q}_t(\underline{\Psi}(t_k), t_k) \tag{23}$$

where:

$$\underline{\Psi}(t_k) = \begin{bmatrix} \varepsilon_O(t_k) \\ \chi_y(t_k) \end{bmatrix} ; \; \underline{Q}_0 = \begin{bmatrix} N_0 \\ M_0 \end{bmatrix} ; \; \underline{Q}_t(\underline{\Psi}(t_k), t_k) = \begin{bmatrix} N_t(\underline{\Psi}(t_k), t_k) \\ M_t(\underline{\Psi}(t_k), t_k) \end{bmatrix}$$

$$\underline{\underline{K}}(\underline{\Psi}(t_k), t_k) \;=\; E_k^* \cdot \begin{bmatrix} K_{11}(\underline{\Psi}(t_k), t_k) & K_{12}(\underline{\Psi}(t_k), t_k) \\ K_{21}(\underline{\Psi}(t_k), t_k) & K_{22}(\underline{\Psi}(t_k), t_k) \end{bmatrix}$$

$$K_{11}(\underline{\Psi}(t_k), t_k) \;=\; \left[\sum_{j=1}^{m} \delta_{kj} \cdot A_{cj} + \sum_{i=1}^{n} \frac{E_r^{\mathrm{sec}}(\varepsilon_{ri}(t_k))}{E_k^*} A_{ri} \right]$$

$$K_{12}(\underline{\Psi}(t_k), t_k) \;=\; K_{21}(\underline{\Psi}(t_k), t_k) \;=\; \left[\sum_{j=1}^{m} \delta_{kj} \cdot A_{cj} \cdot y_{ci} + \sum_{i=1}^{n} \frac{E_r^{\mathrm{sec}}(\varepsilon_{ri}(t_k))}{E_k^*} A_{ri} \cdot y_{ri} \right]$$

$$K_{22}(\underline{\Psi}(t_k), t_k) \;=\; \left[\sum_{j=1}^{m} \delta_{kj} \cdot A_{cj} \cdot y_{ci}^2 + \sum_{i=1}^{n} \frac{E_r^{\mathrm{sec}}(\varepsilon_{ri}(t_k))}{E_k^*} A_{ri} \cdot y_{ri}^2 \right]$$

$$N_t(\underline{\Psi}(t_k), t_k) \;=\; \sum_{j=1}^{m} \delta_{kj} \cdot \sigma_c^*(y_j, t_k) \cdot A_{cj} ; \quad M_t(\underline{\Psi}(t_k), t_k) \;=\; \sum_{j=1}^{m} \delta_{kj} \cdot \sigma_c^*(y_j, t_k) \cdot A_{cj} \cdot y_j \tag{24}$$

The solution of Eq. (23) requires a step by step analysis in which at each time step all the previous stress and strain history has to be known. Because of the non-linear behaviour of concrete an iterative method to compute $\underline{\Psi}(t_k)$ at each time-step has to be inserted in the step by step analysis. The test on convergence of the iterative process is made by verifying that the diagonal terms of the stiffness matrix (large values, independent of the Cartesian coordinate system) become almost invariant.

Once vector $\underline{\Psi}(t_k)$ has been determined, strains follow from Eq. (20) and stresses from Eq. (18), 1 and 2.

Remembering that $\varepsilon_{\sigma 0}(t)$ is due to creep and shrinkage of concrete, the residual strain of the j-th strip of concrete at time t_k (when unloading) can be computed by means of:

$$\varepsilon_{\sigma 0}(y_j, t_k) = \sigma_c(y_j, t_0) \cdot J(t_k, t_0)$$

$$+ \sum_{i=1}^{k-1} \frac{\sigma_c(y_j, t_{i+1}) - \sigma_c(y_j, t_i)}{2} \cdot \sum_{j=1}^{2} P_j \cdot J(t_k, t_{ij}) + \varepsilon_{sh}(t_k) - \frac{\sigma_c(y_j, t_k)}{E_c(t_k)} \tag{25}$$

Note that when dealing for instance with a RC symmetrical (shape and reinforcement) section axially loaded with a long-term compression force Eq. (25) holds for $\varepsilon_{\sigma 0}(y_j, t_k) > 0$ even if $\varepsilon_{sh}(t_k) = 0$, and therefore concrete cracks at unloading because of the elastic response of the rebars.

Owing to the softening branch of the constitutive law of concrete, the load-carrying capacity of the cross section under an instantaneous load increase corresponds to a strain distribution in which no one of the materials has still reached its ultimate strain. A consequence of this statement is that the set of the deformed shapes of the cross section that describe the maximum load-carrying capacities under various combinations of internal actions (hereafter named interaction diagram) is not known, contrary to what happens when dealing with a parabola-rectangle diagram. The interaction diagram has therefore to be determined by means of a step-by-step analysis under increasing values of the internal actions. The solution of the problem is achieved by computing the moment-curvature diagrams under constant eccentricity of the axial force (as already discussed).

Substituting Eqs. (20), 1, 2 and 10 into Eq. (19) at time t (that is at time of instantaneous loading up to ultimate) one obtains:

$$\underline{\underline{K}}(\underline{\Psi}(t)) \cdot \underline{\Psi}(t) = \underline{Q} + \underline{Q}_{\sigma 0}(\underline{\Psi}(t)) \tag{26}$$

where N is the instantaneous axial force acting with eccentricity e ($M = N \cdot e$) and:

$$\underline{\Psi}(t) = \begin{bmatrix} \varepsilon_O(t) \\ \chi_y(t) \end{bmatrix} \quad ; \quad \underline{Q} = \begin{bmatrix} N \\ M \end{bmatrix}$$

$$\underline{\underline{K}}(\underline{\Psi}(t)) = \begin{bmatrix} K_{11}(\underline{\Psi}(t)) & K_{12}(\underline{\Psi}(t)) \\ K_{21}(\underline{\Psi}(t)) & K_{22}(\underline{\Psi}(t)) \end{bmatrix}$$

$$K_{11}(\underline{\Psi}(t)) = \left[\sum_{j=1}^{m} E_c^{sec}(\varepsilon_c(y_j, t) - \varepsilon_{\sigma 0}(y_j, t)) \cdot A_{cj} + \sum_{i=1}^{n} E_r^{sec}(\varepsilon_{ri}(t)) \cdot A_{ri} \right]$$

$$K_{12}(\underline{\Psi}(t)) = K_{21}(\underline{\Psi}(t)) = \left[\sum_{j=1}^{m} E_c^{\text{sec}}(\varepsilon_c(y_j, t) - \varepsilon_{\sigma 0}(y_j, t)) \cdot A_{cj} \cdot y_j + \sum_{i=1}^{n} E_r^{\text{sec}}(\varepsilon_{ri}(t)) \cdot A_{ri} \cdot y_{ri} \right]$$

$$K_{22}(\underline{\Psi}(t)) = \left[\sum_{j=1}^{m} E_c^{\text{sec}}(\varepsilon_c(y_j, t) - \varepsilon_{\sigma 0}(y_j, t)) \cdot A_{cj} \cdot y_j^2 + \sum_{i=1}^{n} E_r^{\text{sec}}(\varepsilon_{ri}(t)) \cdot A_{ri} \cdot y_{ri}^2 \right]$$

$$\underline{Q}_{\sigma 0}(\underline{\Psi}(t)) = \begin{bmatrix} \sum_{j=1}^{m} \varepsilon_{\sigma 0}(y_j, t) \cdot E_c^{\text{sec}}(\varepsilon_c(y_j, t) - \varepsilon_{\sigma 0}(y_j, t)) \cdot A_{cj} \\ \\ \sum_{j=1}^{m} \varepsilon_{\sigma 0}(y_j, t) \cdot E_c^{\text{sec}}(\varepsilon_c(y_j, t) - \varepsilon_{\sigma 0}(y_j, t)) \cdot A_{cj} \cdot y_j \end{bmatrix} \tag{27}$$

The moment-curvature diagram can therefore be computed by means of a step-by-step analysis where at each step the value $\chi_y(t)$ of the curvature is set (starting from the final value given at time t by the long-term analysis) and the values of $\varepsilon_O(t)$ and N are the unknowns. By moving the origin of the axes at distance $y = e$, the unknown N disappears in the second of the equilibrium equations that can therefore be solved by means of an iterative method to determine $\varepsilon_O(t)$. Unknown N can then be computed by replacing $\varepsilon_O(t)$ in the first of the equilibrium equations. This method does not apply to pure bending when $N \cdot e$ is replaced by M whereas $N = 0$. In this case the first of the equilibrium equations can be solved first to determine $\varepsilon_O(t)$, that replaced into the second one allows to compute M.

4. Parametric analysis

The mechanical properties of the materials (nominal values) adopted for the reinforcement are listed in Table 2.

The mean strength of concrete at 28 days $f_{cm}(28)$ is 20 [N/mm^2] (C12) or 58 [N/mm^2] (C50). These two values are the lower and upper bound set by the European code for normal strength concrete.

The home temperature is 20°C and the relative humidity is 60% (usually a lower bound, at least in Europe, when the temperature is about 20°C).

Table 2 Mechanical properties of the rebars adopted in the analysis

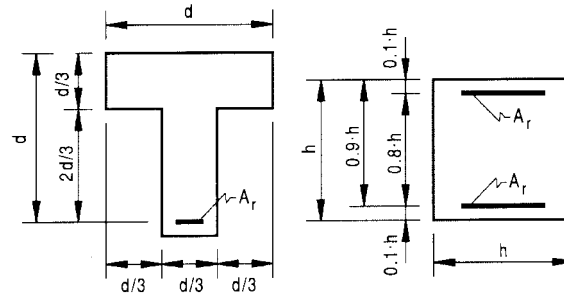|		Steel Fe500 (EURONORM 80-85)	CFRP Leadline® (Mochida *et al.* 1992)	GFRP Isorod® (Challal *et al.* 1993)
Tension characteristics	Strength f_y or f_{Ft} [MPa]	500	1800	700
	Elastic modulus [GPa]	200	147	40
	Ultimate strain ε_{su} or ε_{Fut}	0.12	0.0122	0.0175
Compression characteristics	Strength f_y or f_{Fc} [MPa]	500	>588	520
	Elastic modulus [GPa]	200	147	40
	Ultimate strain ε_{Fut}	-	>0.004	0.0130

Fig. 4 The cross sections adopted in the parametric analysis

A T shape has been adopted to analyse the behaviour of RC sections under pure bending, whereas a square section with symmetric reinforcement has been investigated under bending and compression (see Fig. 4). These shapes underline ductility of the cross sections reinforced with steel and hence magnify the difference with respect to sections reinforced with FRP.

When dealing with the T beam, reinforced with steel, the tensile reinforcement mechanical ratio $\omega = (f_r \cdot A_r)/(f_{cm}(t_0) \cdot A_c) = (f_y \cdot A_s)/(f_{cm}(t_0) \cdot A_c)$ is 0.05, 0.1, 0.15, 0.2, 0.25, 0.3, 0.35, whereas when referring to the square section 0.1, 0.2, 0.4, 0.6 have been adopted instead. These values cover a wide range of cases that can occur in common practice.

An equivalence rule is needed to set the area of the FRP reinforcement. The main problem is that FRP reinforcement has a strength higher than that of steel but a lower elastic modulus. If the equivalence is made with respect to the ultimate tensile force (that is $f_y \cdot A_s = f_{Ft} \cdot A_F$), the area computed for the CFRP reinforcement is very small (about 1/3.5) and hence the stiffness of the RC cracked member under service loads is very small. On the contrary, if the equivalence is made with respect to the stiffness of the reinforcement (that is $E_s \cdot A_s = E_{Ft} \cdot A_F$) when dealing with GFRP the area of the reinforcement can be enormous. Hence, it was decided to adopt the same areas already set for steel reinforcement (underlined in the figures through the geometrical reinforcement ratio $\rho_i = A_r/A_c$). This choice implies that both stiffness under service loads and strength of similar sections reinforced with these three materials cannot be directly compared.

In all, 66 RC cross sections have been analysed.

The moment-curvature diagrams of the T cross sections cast with a C12 concrete are represented in Fig. 5. Those related to C50 concrete are represented in Fig. 6.

These diagrams show a residual positive curvature at unloading. This is because of the combined effect of the reinforcement placed only at the lower layer of the cross section and of shrinkage of concrete (this does not occur when dealing with the square sections that have rebars placed also in the compression zone). This outcome can be clearly understood when looking at Fig. 7 where the stress and strain distribution before and after long-term loading are drawn together with $\varepsilon_{\sigma 0}(t)$. The dashed line represents the total strain $\varepsilon(t)$ at unloading. Owing to the lack of strength of concrete under tension, it is not the only solution, but it is the first one that gives a zero stress resultant when unloading.

The same figure shows that the stress distribution, that is almost linear at time t_0 (owing to the small stresses acting at this stage), becomes non linear after long-time loading. The compressed zone widens with time (see Mola and Gattesco 1983). This zone can be divided in three parts. The upper part (zone 1 in Fig. 7) is the one always under compression. There the stress distribution is
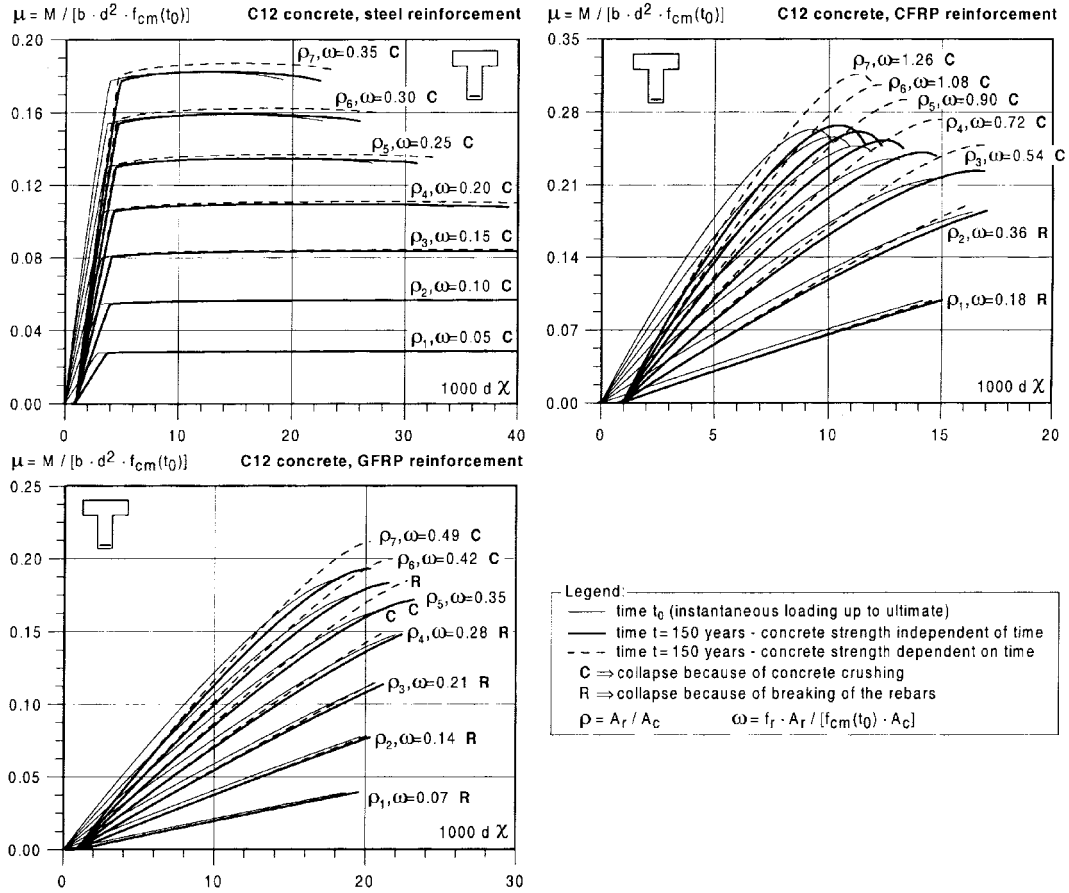
Fig. 5 Moment-curvature diagrams of the T cross sections made with C12 concrete

almost linear also after long-time loading (instantaneous stresses almost linear and linear visco-elasticity). In the middle one (zone 2) each concrete layer becomes compressed at distinct times τ between time at first loading t_0 and actual time t, and creep starts to affect the stress in that layer from time τ on. In the lower zone (zone 3) in spite of a compressive total strain, the stress is zero because of the effect of shrinkage.

Figs. 5 and 6 show that if steel reinforcement is yielded at ultimate and concrete strength is kept constant, the load-carrying capacity of the cross section does not change because of creep and shrinkage of concrete (a result already well established).

When taking into account the strength increase (because of continued hydration) of concrete, the load-carrying capacity of the cross section increases. The compressive stress resultant at ultimate has nevertheless to be equal to the tensile stress resultant, that is to the resultant strength of the rebars $(f_s \cdot A_s)$ if the reinforcement has yielded. Therefore, the compressive stress resultant (at ultimate) cannot change (it is once again independent of creep and shrinkage of concrete), and the load-carrying capacity increase depends just on the increase of the lever arm (owing to the reduction of the compressed zone of the cross section at ultimate). Consequently, the load-carrying capacity increase is proportional to the area of the steel reinforcement, but it is anyway much lower than the

$\mu = M / [b \cdot d^2 \cdot f_{cm}(t_0)]$ **C50 concrete, steel reinforcement**

$\mu = M / [b \cdot d^2 \cdot f_{cm}(t_0)]$ **C50 concrete, CFRP reinforcement**

$\mu = M / [b \cdot d^2 \cdot f_{cm}(t_0)]$ **C50 concrete, GFRP reinforcement**

Legend:
— time t_0 (instantaneous loading up to ultimate)
— time $t = 150$ years - concrete strength independent of time
- - - time $t = 150$ years - concrete strength dependent on time
C $\Rightarrow$ collapse because of concrete crushing
R $\Rightarrow$ collapse because of breaking of the rebars
$\rho = A_r / A_c$ $\omega = f_r \cdot A_r / [f_{cm}(t_0) \cdot A_c]$
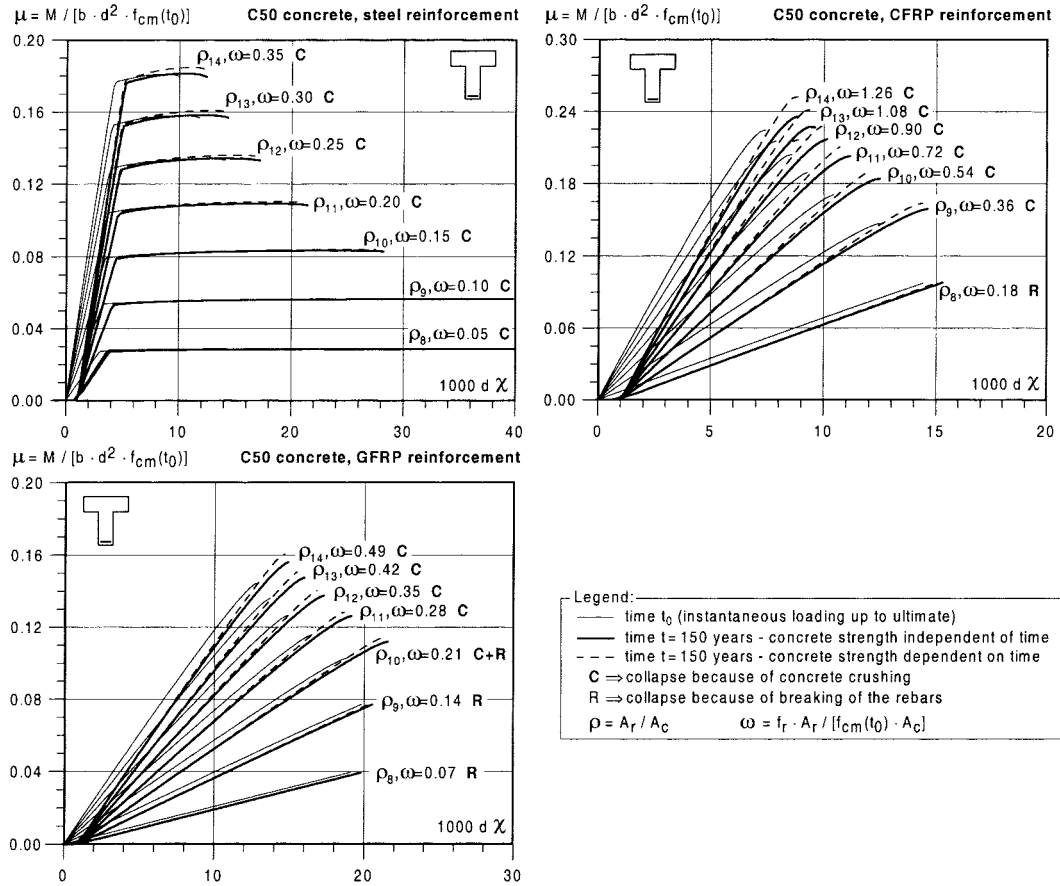
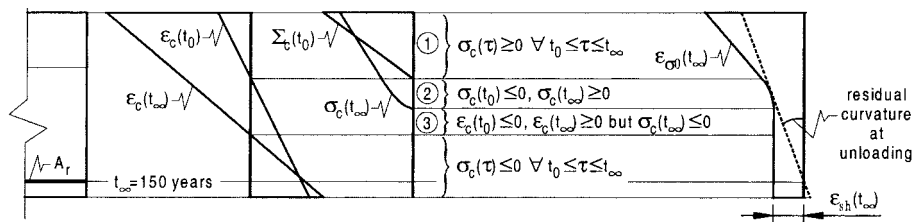Fig. 6 Moment-curvature diagrams of the T cross sections made with C50 concrete

Fig. 7 Stresses and strains before and after long-term loading

concrete strength increase (looking at the diagram with $\omega = 0.35$ in Fig. 5, the cross section load-carrying capacity increase is equal to 2.56%, whereas the strength increase of concrete is about 25%).

Owing to the adoption of a realistic ultimate strain of steel (that is 0.12), collapse of the bent sections reinforced with steel always occurs because of concrete crushing. When adopting the minimum reinforcement suggested by the codes (about $\omega = 0.05$), the reinforcement of the T section yields. From this point on, its strain grows up to about 0.1 without increasing the tensile stress resultant but markedly reducing the depth x^* of the neutral axis, that is the compressed zone

that at last crushes.

The ultimate strain of the FRP rebars is about 1/10 of that of steel and x^* is much higher, hence collapse can occur because of breaking of the rebars if the reinforcement ratio is small, or because of concrete crushing if it is higher. The curvature at ultimate of the sections reinforced with steel is anyway much higher (up to 500%) than that of the sections reinforced with FRP, especially when referring to small reinforcement ratios, that is where the strain of the reinforcement at ultimate is higher.

Contrarily to what has been stated for traditional sections reinforced with steel, creep and shrinkage of concrete affect the load-carrying capacity of the sections reinforced with FRP. On one hand, if collapse occurs because of breaking of the rebars, this effect is very small both when keeping the concrete strength constant with time and when taking into account its increase because of continued hydration. On the other hand, if collapse occurs because of concrete crushing, this effect is much more significant. The outcomes of the analyses made with constant strength of concrete show that this increase is maximum (8.82% at $\omega = 0.28$) for high strength of concrete (C50) and GFRP, minimum for low strength of concrete (C12) and CFRP. When taking into account the strength increase of concrete, the load-carrying capacity of the cross section increases much
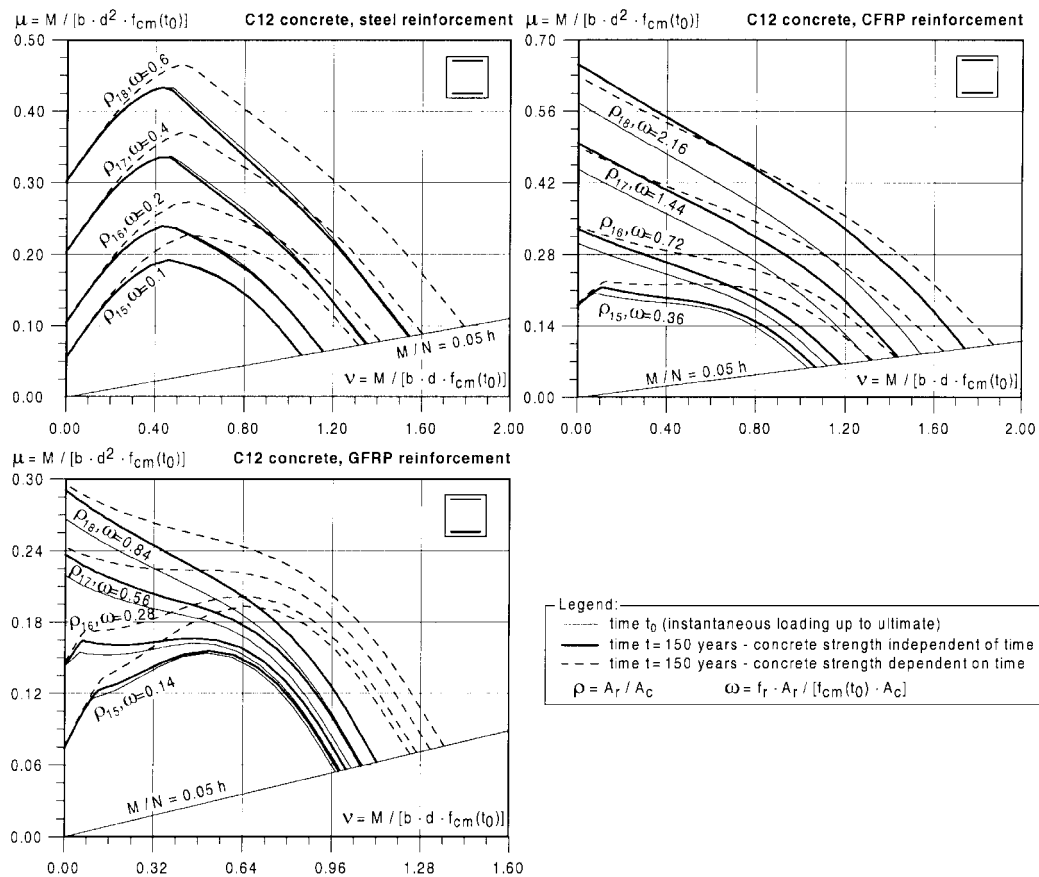

Fig. 8 Interaction diagrams of the square cross sections made with C12 concrete
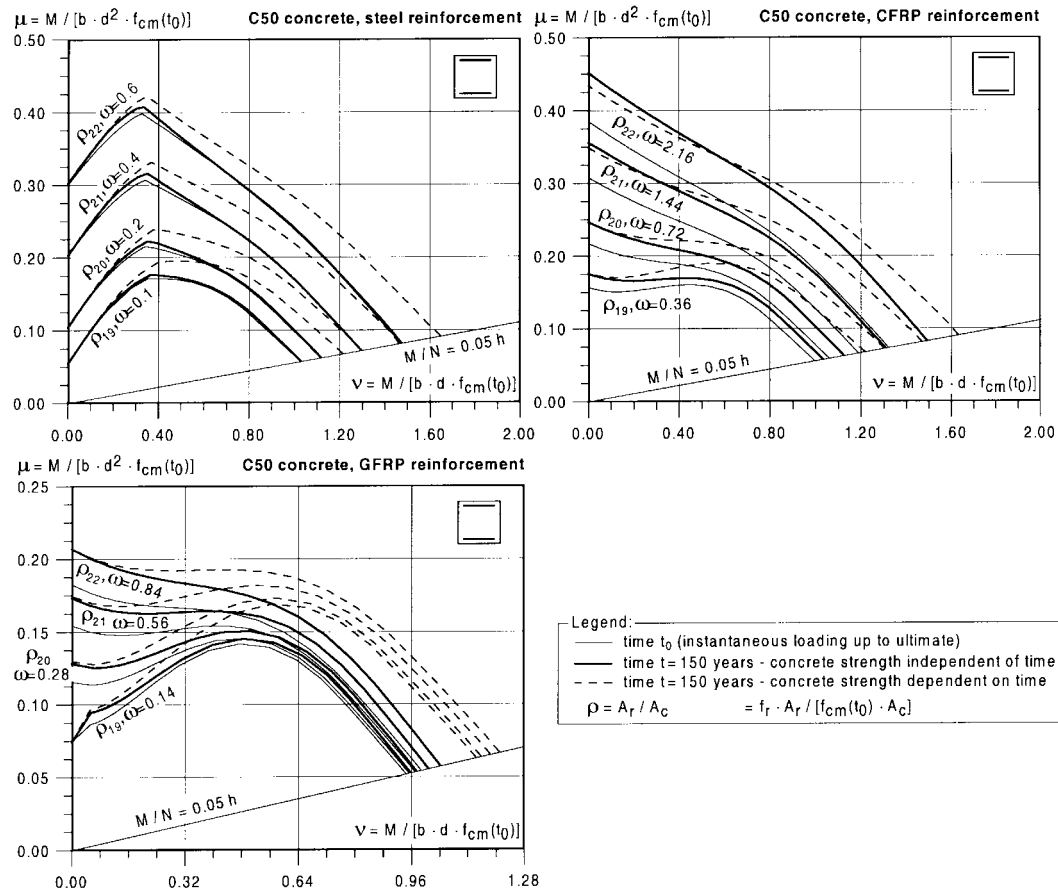
Fig. 9 Interaction diagrams of the square cross sections made with C50 concrete

more (up to 20.05%), contrarily to what happens when dealing with steel rebars.

Figs. 8 and 9 show the interaction diagrams of the rectangular sections. The diagrams that refer to the sections reinforced with steel show once more that under pure bending creep and shrinkage of concrete do not affect the load-carrying capacity of the section (if strength of concrete is constant) and that a marked strength increase of concrete slightly affects it. When increasing the ultimate axial force things do not markedly change if concrete strength is kept constant (the maximum difference gathered between the instantaneous load-carrying capacity and the one related to instantaneous overloading after long-term loading is 2% for both C12 and C50 concrete). A strength increase of concrete means an increase of the load-carrying capacity of the section that grows together with the ultimate axial force.

For the sake of completeness, it has to be mentioned that in all the computations made keeping strength of concrete constant, part or all of the reinforcement is yielded at ultimate. Some tests made after increasing the concrete cover as much not to have yielding of the compression reinforcement (very unusual in common practice), gave results similar to those already stated for a concrete strength increase.

The interaction diagrams regarding the rectangular sections reinforced with FRP are quite different

from the previous ones. Usually collapse occurs because of concrete crushing but if the reinforcement ratio is small, collapse can occur because of breaking of the rebars. If so, the interaction diagram shows a corner that represents collapse both of concrete and of the tension rebars. When collapse occurs because of breaking of the rebars, the more the maximum strain in concrete is far from ultimate, the less the load-carrying capacity of the cross section increases. When collapse occurs because of concrete crushing and the strength of concrete does not change with its age, the increase of the load-carrying capacity of the cross section is almost constant, up to 15%. An increase of the strength of concrete with its age means a marked increase of the load-carrying capacity of the section, higher if dealing with high values of the ultimate axial force.

5. Conclusions

A method to compute the load-carrying capacity of compact cross sections that are at first submitted to a constant long-term service load and then instantaneously overloaded up to ultimate is presented. This method couples the instantaneous and delayed constitutive laws of concrete and shows a way to perform at first the non-linear visco-elastic analysis, then the non-linear analysis up to ultimate that takes into account the self-equilibrated stress distribution previously computed.

The parametric analysis performed with this method allows one to verify that creep and shrinkage of concrete do not change the load-carrying capacity of RC sections reinforced with steel rebars if the strength of concrete is kept constant. This does not occur when dealing with FRP rebars. Anyway, no reduction of the load-carrying capacity appeared from the calculations. This outcome can be justified by stating that creep reduces the maximum compressive stresses in concrete and hence usually improves the capability of the most compressed layer of the section to resist compressive stress increases. This effect is important if the rebars have an elastic behaviour at ultimate and vanishes if they have markedly yielded.

The previous outcomes that refer to FRP rebars demonstrated to apply:
- whatever the strength of concrete is;
- whether the strength increase of concrete with its age is taken into account or not;
- whatever the strength, the elastic modulus and the area of the FRP reinforcement are.

All the previous remarks, together with the observations that:
- even when dealing with steel reinforcement the load-carrying capacity of the cross section markedly increases if the strength of concrete is not kept constant (see Figs. 5, 6, 8 and 9);
- the loading history (i.e., the combination of the long-term internal actions and the way these actions instantaneously increase up to ultimate) affects the result when dealing with bending and compression. As a matter of fact it has been stated that the self-equilibrated stress distribution owing to creep affects the load-carrying capacity of compact cross section reinforced with FRP rebars, but this self-equilibrated stress distribution depends on the combination of the long-term internal actions that do not necessarily proportionally increase in practice when approaching the ultimate load.
- the maximum load-carrying capacity increase computed for sections reinforced with FRP (and constant compressive strength of concrete) is 15% (in unfavourable environment and long-term load conditions);
- a simple and protective rule has anyway to be added to the codes to allow the adoption of FRP rebars;

lead, at present, to suggest not to take into account in common practice the increase of the load-carrying capacity of the cross section owing to the self-equilibrated stress distribution related to the delayed behaviour of concrete.

An explanation of this statement derives from a comparison with the analysis of slender RC columns. In spite of the possibility of performing a refined and reliable computation of the load-carrying capacity of these columns, the needs of common practice, together with the uncertainties (related for instance to the forecast of the position of "local faults" in the column) led the authors of the European code to suggest not to take into account the second order effects if the reduction of the load-carrying capacity of the column is lower than 10% (CEN 1991), even though this suggestion is not conservative. Most of the outputs of the analyses already done (with constant strength of concrete) show an increase of the load-carrying capacity of the section lower than 10% and the choice not to take it into account is conservative. Besides, the error gathered by both the American and European codes with respect to the experimental tests, in the computation of shear strength of beams, is often greater than 15%.

It is anyway important to state that the assumption that the load-carrying capacity of RC sections reinforced with FRP rebars be kept constant all over the intended life of the structure is only an approximation, whereas it is more accurate when dealing with steel rebars.

A more in depth knowledge of the mechanical and rheological behaviour of the materials adopted could lead to more refined design rules, but practical applications can not wait for an exhaustive knowledge of all the aspects related to the problem.

Acknowledgements

References

Agarwal, B.D. and Broutman, L.J. (1994), *Analysis and Performance of Fiber Composites*, Wiley Interscience.
ASTM (1992), *Standard Test Method for Compressive Properties of Rigid Plastics*, ASTM D695M-91, American Society for Testing and Materials, Philadelpia, Pa., Vol. 08.01.
Benmokrane, B. and Chaallal, O. (1996), "Fiber-reinforced plastic rebars for concrete applications", *Composites. Part B: Engineering*, **27B**.
CEB (1984), CEB Design Manual on Structural Effects of Time-dependent Behaviour of Concrete, *CEB Bulletin d'Information N° 142/142bis*, Lausanne, Switzerland.
CEB-FIP (1991), CEB-FIP Model Code 1990, *CEB Bulletin d'Information N°203-204-205*, Lausanne, Switzerland.
CEB (1993), Selected Justification Notes, *CEB Bulletin d'Information N° 217*, Lausanne, Switzerland.
CEE (1986), "Acciaio per armature per cemento armato non precompresso", *EURONORM 80-85*.
CEN (1991), *Eurocode n.2: Design of Concrete Structures - Part 1: General Rules and Rules for Buildings, ENV 1992-1-1*, European Committee for Standardization, Commission of the European Communities, Brusselles, Belgium.
Chaallal, O. and Benmokrane, B. (1993), "Physical and mechanical performance of an innovative glass-fiber reinforced plastic rod for concrete and granted anchorages", *Canadian Journal of Civil Engineering*, **20**(2), 254-268.
Erki, M.A. and Rizkalla, S.H. (1993), "FRP reinforcement for concrete structures", *Concrete International, American Concrete Institute*, **15**(6), 48-53.

Jung, T.H. and Subramanian, R.V. (1994), "Alkali resistence enhancement of basalt fibers by hydrated zirconia films formed by the sol-gel process", *J. Mater. Res.*, **9**(4), 1006-1013.

Machida, A., Tanaka, T. and Yagi, K. (1992), "The development and application of a ground anchor using new materials", *Advanced Composite Materials in Bridges and Structures*, K. W. Neale and P. Labossière Editors, Canadian Society for Civil Engineering, 393-402.

Machida, A. Editor (1993), *State-of-the-art Report on Continuous Fiber Reinforcing Materials*, Japan Society of Civil Engineering, Tokyo, Japan.

Malvar, L.J. (1994), "Unidirectional, core-shell hybrids for concrete reinforcement - A preliminary study", *Naval Facilities Engineering Service Center,* Port Hueneme (CA, USA), **TR-2011-SHR**.

Mola, F. and Gattesco, N. (1983), "Creep effects in RC cracked sections", *Proc. Theoretical and Applied Mecanics Department*, University of Udine (in Italian).

Nanni, A. Editor (1993), *Fiber-Reinforced-Plastic (FRP) Reinforcement for Concrete Structures: Properties and Applications*, Elsevier.

Pisani, M.A. (1994), "Numerical analysis of creep problems", *Computers & Structures*, **51**(1), 57-63.

Pisani, M.A. (2000), "Long-term behaviour of beams prestressed with aramid fibre cables - Part 1: a general method", *Engineering Structures*, **22**(2000), 1641-1650.

Pisani, M.A. (1996), "A numerical method to analyse compact cross sections", *Computers & Structures*, **59**(6), 1063-1072.

Rotter, J.M. (1985), "Rapid exact inelastic biaxial bending analysis", ASCE *J. Struct. Eng.*, **111**(12), 2659-2674.

Tepfers, R., Tamuzs, V., Apinis, R. and Modniks, J. (1999), "Pull-out, flexural rotation capacity and creep tests using hybrid composite rods and CFCC rods for reinforcement in concrete", Chalmers University of Technology, Division of Building Technology, Work No.32, Publication 99:4, Göteborg, Sweden.

Notations

The following symbols are used in this paper:

A	: area
E	: Young modulus
e	: eccentricity = M/N
P	: external load
f	: strength (of a material)
$\underline{K}$	: stiffness matrix
J	: creep function
M	: bending moment
m	: number of strips that discretize the cross section
N	: axial force
n	: number of the rebars of the cross section
$\underline{Q}$	: vector of the internal actions or of equivalent internal actions
t	: age of concrete (without subscript 0 it is the actual age of concrete)
x^*	: depth of the neutral axis
χ	: curvature
ε	: strain (compression is positive)
$\varepsilon_{\sigma 0}$	: residual strain after instantaneous unloading
φ	: creep coefficient
ρ	: geometrical reinforcement ratio
σ	: normal stress (compression is positive)
τ	: time between time t_0 and time t
ω	: reinforcement mechanical ratio
$\underline{\Psi}$	: vector of the unknowns

Subscripts

F	: fibre reinforced polymer
Ft	: fibre reinforced polymer, tensile stress
Fc	: fibre reinforced polymer, compressive stress
c	: concrete
inst	: instantaneous
m	: mean value
O	: origin of the cartesian axes
r	: rebar
s	: mild reinforcing steel
sh	: shrinkage
y	: yielding
u	: ultimate
0	: at first loading

Superscripts

sec	: secant
tg	: tangent